Formation of active sites and hydrodesulfurization activity of rhodium phosphide catalyst: Effect of reduction temperature and phosphorus loading

Formation of active sites and hydrodesulfurization activity of rhodium phosphide catalyst: Effect of reduction temperature and phosphorus loading

doi: info:doi/10.1016/j.apcata.2014.01.049

Highlights

► The Rh-1.5P catalyst exhibited the highest activity among the investigated catalysts.

► Rh_2P was easily formed in catalysts with a higher P loading.

► Higher P loadings and higher reduction temperatures led to aggregation of Rh species.

► RhP_2 exhibits lower catalytic activity than Rh_2P.

► High HDS activity was caused by small Rh_2P formation at lower reduction temperature.

Graphical abstract

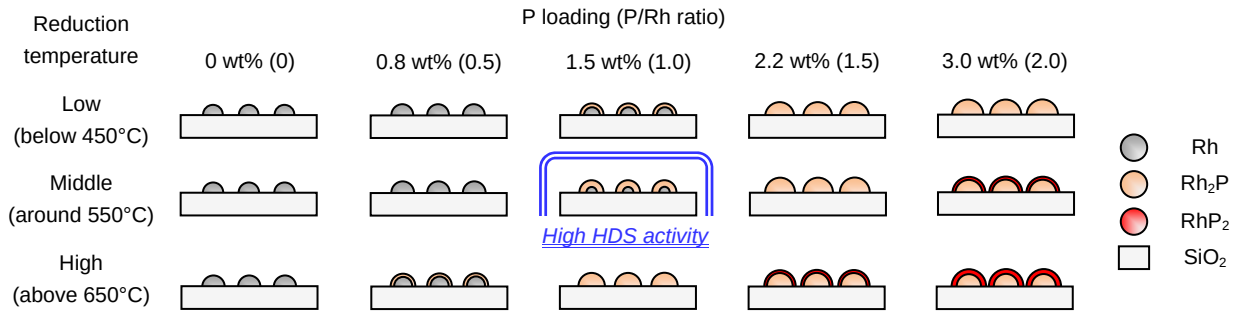

Formation of Active Sites and Hydrodesulfurization Activity of Rhodium Phosphide Catalyst: Effect of Reduction Temperature and Phosphorus Loading

Yasuharu Kanda[a*], Chisato Temma[b], Ayaka Sawada[c], Masatoshi Sugioka[d], and Yoshio Uemichi[a]

[a]Applied Chemistry Research Unit, College of Environmental Technology, Graduate School of Engineering, Muroran Institute of Technology, 27-1 Mizumoto, Muroran 050-8585, Japan

[b]Division of Applied Chemistry, Graduate School of Engineering, Muroran Institute of Technology, 27-1 Mizumoto, Muroran 050-8585, Japan

[c]Division of Chemical and Materials Engineering, Graduate School of Engineering, Muroran Institute of Technology, 27-1 Mizumoto, Muroran 050-8585, Japan

[d]Aeronautics and Astronautics Unit, College of Design and Manufacturing Technology, Graduate School of Engineering, Muroran Institute of Technology, 27-1 Mizumoto, Muroran 050-8585, Japan

Abstract

Effects of reduction temperature and phosphorus loading on rhodium phosphide (Rh_2P) formation and on the catalytic activity of Rh-xP catalysts for hydrodesulfurization (HDS) were investigated to prepare highly active HDS catalysts. Analysis of the Rh-xP catalysts showed that a suitable P loading for HDS activity is 1.5 wt%—four times greater than that of an Rh catalyst. Temperature-programmed reduction and X-ray diffraction analyses of the Rh-xP catalysts showed that Rh_2P is readily formed in catalysts with higher P loading. In contrast, the results of transmission electron microscopy observation and CO adsorption experiments indicated that the Rh_2P particle size increased with increasing P content. Thus, the high HDS activity of the Rh-1.5P catalyst was explained by the formation of small Rh_2P at a relatively low reduction temperature (550 °C).

Keywords

Rhodium phosphide catalyst; Hydrodesulfurization; Phosphorus loading; Reduction temperature; Active site formation

1. Introduction

During the past decade, the development of technologies capable of solving environmental problems such as acid rain and global climate change have attracted substantial attention on a global scale. The combustion of organic sulfur compounds in fuels used for boilers and engines results in the formation of sulfur oxides (SO_X). SO_X causes acid rain and deactivates automotive exhaust catalysts. Regulation of SO_X emissions from ships is expected to become more stringent because the fuels for ships contain greater quantities of sulfur compounds compared to gasoline and diesel fuel. Thus, the petroleum industry has been producing clean fuels via hydrodesulfurization (HDS) processes that use sulfided Co(Ni)Mo/Al_2O_3 catalysts. Recently, the petroleum industry claimed that the development of highly active HDS catalysts that exhibit greater activity than commercial CoMo catalysts will prevent acid rain and the deactivation of automotive exhaust catalysts [1-3].

Methods of preparing highly active CoMo-based HDS catalysts, such as the Co chemical vapor deposition technique [4, 5] and the addition of citric acid [6] or phosphorus [5, 7, 8], have been widely investigated.

Furthermore, new active phases other than sulfided CoMo catalysts have been reported by numerous researchers. Noble metals [9-14] and transition-metal carbides [15-18], nitrides [15, 19], and phosphides [2, 3, 18, 20-40] have been used as new HDS catalysts, and new transition-metal phosphides such as Ni_2P [2, 3, 18, 20-31] and MoP [30-35] have received extensive attention [30]. In particular, Ni_2P catalysts have demonstrated high potential for use in the HDS reaction. Reports have described the effects of P loading on the formation of the nickel phosphide phase and on the catalyst's HDS activity. The reduction of precursors that contain less P is known to proceed via the $Ni_{12}P_5$ phase, which is an intermediate in the formation of Ni_2P [35]. In addition, the reduction of precursors with higher P concentrations results in the formation of the Ni_2P phase [20, 21, 25, 29]. The optimal P/Ni ratio for HDS activity was found to be 0.8–2.2, which is greater than the stoichiometric P/Ni ratio in Ni_2P (0.5). However, we [37-39] and Bussell et al. [3, 40] have reported that rhodium phosphide (Rh_2P) supported on SiO_2 exhibits high and stable catalytic activity toward the HDS reaction. As with the Ni_2P catalysts, the P/Rh ratio should also strongly affect the

formation of Rh_2P and the HDS activity of Rh catalysts. Previously, we reported that the support strongly affects the formation of Rh_2P and its HDS activity and that SiO_2, TiO_2, and Al_2O_3 supports showed superior HDS activity compared to MgO and ZrO_2 supports [38]. However, the formation of Rh_2P on Al_2O_3 is difficult because of the formation of $AlPO_4$ [3], and the turnover frequency (TOF) of Rh_2P is remarkably enhanced by the interaction between the active phase and TiO_2 [38]. Thus, SiO_2, which does not exhibit a strong interaction with Rh_2P or P when used as a support, is a superior support for clarifying the effects of the P loading on Rh_2P formation and on its catalytic HDS activity. As previously noted, numerous reports have described the effects of P loadings on the formed phases and on their HDS activities. However, the effect of P loading on the reducibility of phosphates and on the formation temperature of phosphides, especially noble metal phosphides, has scarcely been reported. In addition, reduction temperature is one of the most important factors in evaluating the reducibility of phosphates and the formation of phosphides. Herein, the effects of reduction temperature and P loading on the formation of rhodium phosphides (Rh_XP_Y) and on the HDS activity of

Rh_2P/SiO_2 catalysts were examined to enable the preparation of highly active phosphided HDS catalysts.

2. Experimental

2. 1. Catalyst preparation

Silica (SiO_2, BET surface area 295 $m^2\ g^{-1}$) was supplied by Nippon Aerosil Co. The Rh/SiO_2 catalyst was prepared by an impregnation method described previously [37-39]. Rhodium(III) chloride trihydrate ($RhCl_3 \cdot 3H_2O$, Kanto Chemical Co.) was used as a precursor for the catalysts and was dissolved in water. The Rh loading amount was 5 wt%. After impregnation, the catalyst was dried at 110 °C for 24 h, followed by heat treatment under nitrogen (N_2) stream at 450 °C for 1 h in order to decompose the Rh salts. The sieved catalysts (30- to 42-mesh-size granules) were calcined in air at 500 °C for 4 h. The ramp rate for the heat treatment and calcination was 10 °C min^{-1}. P-added 5 wt% Rh (Rh-P)/SiO_2 catalysts were prepared using the same procedure, except with aqueous solutions of $RhCl_3 \cdot 3H_2O$ and ammonium dihydrogen phosphate ($NH_4H_2PO_4$, Kanto Chemical Co.). The P concentration was

varied from 0.8 to 3.0 wt%. These catalysts were labeled as Rh-xP, where "x" denotes the P loading (wt%). The P/Rh molar ratio in the catalysts with 0.8, 1.5, 2.2, and 3.0 wt% P was 0.5, 1.0, 1.5, and 2.0, respectively.

2. 2. Hydrodesulfurization of thiophene

The HDS of thiophene was performed at 350 °C under 0.1 MPa using a conventional fixed-bed flow reactor. The calcined catalyst (0.1 g) was charged into the quartz reactor and heated (10 °C min^{-1}) in a helium (He) stream (30 ml min^{-1}) at 500 °C for 1 h, following which it was reduced by H_2 (30 ml min^{-1}) at 350–700 °C for 1 h. A hydrogen–thiophene gas mixture (H_2/C_4H_4S = 30), obtained by passing a H_2 stream through a thiophene trap cooled at 0 °C, was then introduced into the reactor (W/F = 37.9 g h mol^{-1}). The reaction products were analyzed using a gas chromatograph equipped with a flame ionization detector (FID) and a silicone DC-550 (length: 2 m, temperature: 110 °C) and Al_2O_3/KCl plot (ID: 0.53 mm, length: 25 m, film thickness: 10 μm, temperature: 60–190 °C, rate: 7.5 °C min^{-1}) columns.

The rate constant was calculated from the following equation under the assumption of a pseudo-first-order reaction:

$$k_{HDS} = \frac{-\ln(1-x/100)}{W/F} \quad (1)$$

where k_{HDS} is the reaction rate of thiophene HDS (mol h^{-1} g^{-1}) and x is the conversion rate at 3 h (%).

2. 3. Catalyst characterization

The Rh and Rh-xP catalysts were characterized using N_2 adsorption, temperature-programmed reduction (TPR), X-ray diffraction (XRD), transmission electron microscopy (TEM), and carbon monoxide (CO) adsorption analyses. Measurements of N_2 adsorption at −196°C were performed using a Micromeritics ASAP 2010. The catalysts were evacuated at 300 °C for 10 h prior to the N_2 adsorption measurements. The surface area of the catalysts was calculated by the Brunauer–Emmett–Teller (BET) method. TPR measurements were performed using a Shimadzu GC-8A gas chromatograph. The supported Rh or Rh-xP catalysts (0.1 g) were heated in a He stream (30 ml min^{-1}) from room temperature to 500 °C at 10 °C min^{-1}, followed by He treatment at 500 °C for 1 h. After this He treatment, the catalysts were cooled to 30°C in a He stream, and the He was switched to a hydrogen–nitrogen (5 vol%H_2-N_2) gas mixture at 30 °C for 0.5 h before

the measurement was performed. The TPR spectrum was recorded over the temperature range of 30 to 800 °C at 10 °C min^{-1}, using a thermal conductivity detector (TCD) to monitor H_2 consumption. Water was removed using a molecular sieve trap. The XRD patterns of the calcined and reduced catalysts in air were measured using a Rigaku MiniFlex equipped with a Cu Kα radiation source operated at 30 kV and 15 mA. The crystallite size of the metallic Rh and Rh_XP_Y were calculated using Scherrer's equation:

$$d = \frac{K\,\lambda}{B\,Cos\theta} \quad (2)$$

where d is the crystallite size (nm), B is the full-width at half maximum of the selected peak (FWHM, radians), K is shape factor (0.9), and λ is the wavelength of the X-ray radiation (15.4184 nm). The XRD peaks at 34.2° (Rh_2O_3, (114) plane), 40.9° (Rh, (111) plane), 46.7° (Rh_2P, (220) plane), and 23.9° (RhP_2, (11-1) plane) were used to calculate the B parameter.

TEM observations were performed using a JEOL JEM-2000FX. The conditions of TEM operation were an acceleration voltage of 200 kV and a magnification of 120,000×. The particle size distribution and average particle size were determined from the measurements of 1000 particles in

the TEM micrographs. The CO uptake of the supported Rh and Rh-P catalysts was measured using the pulse method. The supported Rh or Rh-xP catalysts (0.1 g) were treated in He at 500°C (10 °C min^{-1}) for 1 h, followed by reduction in H_2 at 350–750 °C for 1 h. CO was injected onto the catalyst layer at 25 °C using a sampling loop (1.0 ml). The amount of CO adsorbed was measured with a Shimadzu GC-8A gas chromatograph equipped with a TCD.

3. Results and Discussion

3. 1. HDS of Thiophene over Rh-xP Catalysts

3. 1. 1. HDS Activities of the Rh-xP Catalysts

Previously, we reported that reduction temperature strongly affects the HDS activity of Rh-1.5P catalysts [37-39]. Thus, the HDS activity of Rh-xP catalysts reduced at various temperatures was examined in this work. **Figure 1** shows the effect of reduction temperature on the HDS activity (rate constant) of the Rh-xP catalysts after reaction for 3 h. The HDS activity of the Rh catalyst barely changed with an increase in reduction temperature. In contrast, an optimal reduction temperature for

the maximum HDS activity of the P-added Rh catalysts was clearly observed. The optimal reduction temperature for achieving maximum HDS activity of the Rh-xP catalysts decreased with increasing P content. Moreover, the HDS activity of the catalysts with a 3.0 wt% P loading decreased remarkably with an increase in reduction temperature.

The HDS activity of the Rh-xP catalysts reduced at the optimal temperature is shown in **Fig. 2** as a function of the P loading. The maximum HDS activity for the Rh-xP catalysts was obtained at a P loading of 1.5 wt%. This activity was four times greater than that of the Rh catalyst.

3. 1. 2. Selectivity of Products

The HDS reaction products were butanes, butenes, tetrahydrothiophene (THT), and trace amounts of cracking products. The selectivity for each reaction product in the HDS of thiophene over the Rh-xP catalysts is listed in **Table 1**. Because the selectivities of butanes, butenes, and THT depend on P loading, reduction temperature, and thiophene conversion rate, the effect of the P loading on the product selectivities should be evaluated at the same reduction temperature and

with a similar thiophene conversion rate. The Rh-0.8P and Rh-1.5P catalysts that were reduced at 650 °C exhibited similar conversion rates, where butanes were readily formed on the Rh-xP catalysts with lower P loadings. In contrast, the THT selectivity of the Rh-0.8P catalyst reduced at 650 °C was lower than that of the Rh-1.5P catalyst. The same THT selectivity was trend was observed for the Rh-1.5P and Rh-2.2P catalysts reduced at 450 °C.

Furthermore, the effect of W/F on the product selectivities of Rh and Rh-1.5P catalysts reduced at 650 °C are listed in **Table 2**. At similar conversion rates, THT selectivity increased with increasing P loading, but butans selectivity decreased. Thus, the P loading strongly affected the selectivities for butanes and THT.

3. 2. Characterization of the Rh-xP Catalysts

3. 2. 1. BET Surface Area of the Calcined Rh-xP Catalysts

The surface area of the calcined Rh-xP catalysts is shown in **Table 3**. The Rh catalysts exhibited the same surface area as the SiO_2 support (295 $m^2\ g^{-1}$). The surface area of the Rh-xP catalysts decreased with increasing P loading. However, the surface area was hardly changed when the P

loading was increased from 2.2 to 3.0 wt%. These results indicate that phosphates preferentially interact with the support, but not with Rh species, to aggregate SiO_2 particles.

3. 2. 2. XRD Patterns of the Calcined Rh-xP Catalysts

Figure 3 shows the XRD patterns of the Rh-xP catalysts after calcination at 500 °C. The main peak of Rh_2O_3 was observed in the XRD patterns of the Rh-xP catalysts, and this peak barely changed when the P loading was increased to 1.5 wt%. However, the XRD patterns of the Rh-2.2P and Rh-3.0P catalysts showed remarkably sharp peaks associated with metallic Rh.

The crystallite sizes of the metallic Rh and Rh_2O_3 in the catalysts, as calculated using Scherrer's equation, are also listed in **Table 3**. The crystallite size of the Rh_2O_3 increased with an increase in the P loading. In particular, a large crystallite size was observed in the catalysts with higher P loadings (2.2 and 3.0 wt%). The large metallic Rh particles probably formed during decomposition of the Rh-based salt. Because oxygenation proceeds from the surface to the bulk, a large Rh particle, which has a high diffusion resistance, will remain in the metallic Rh state

after calcination.

3. 2. 3. TPR of the Rh-xP Catalysts

Reduction temperature and P loading strongly affected the HDS activity of the Rh-xP catalysts, as shown in **Figs. 1 and 2**. Therefore, the TPR traces of the Rh-xP catalysts were examined to clarify the effect of the P loading on the reducibility of the rhodium oxide and phosphate species. **Figure 4** shows the TPR trace of the Rh-xP catalysts. The peak at 60°C, which was attributed to the reduction of Rh_2O_3, appeared in the TPR trace of the Rh catalyst (**Fig. 4, (a)**). The peak for Rh_2O_3 reduction was observed from 60 to 140 °C in the TPR trace of Rh-xP catalysts. When the P loading was increased, this peak shifted to a higher temperature. The same trend was observed in the TPR traces for the Ni-P catalysts [21, 24]. The phosphate would cover Rh_2O_3 particles, causing the peak temperature of the Rh_2O_3 reduction to shift. However, the reduction temperature of Rh_2O_3 in the Rh-0.8P catalyst hardly changed compared with that of Rh_2O_3 in the Rh catalyst. These results imply that phosphate preferentially interacts with SiO_2 but not with Rh_2O_3.

The TPR trace of a physically mixed Rh/SiO_2 and 1.5% P/SiO_2 catalyst

(0.05 + 0.05 = 0.1 g) was measured to define the reduction peak of the phosphates (**Fig. 4, (b)**). Two peaks were observed at approximately 50 °C and above 650 °C. In the mixed catalyst, the Rh_2O_3 barely interacted with the phosphate. Thus, these peaks were attributed to the reduction of the Rh_2O_3 and to the phosphates supported on the SiO_2, respectively. However, a reduction peak in the temperature range of 200–350°C was not observed in the trace of the mixed catalyst, indicating that this peak was attributed to the reduction of the phosphate that interacted with the Rh_2O_3.

In the temperature range above 250 °C in the TPR spectrum of the Rh-0.8P catalyst, two peaks were observed at 340 and 800 °C in (**Fig. 4, (b)**). For the Rh-1.5P catalyst, these peaks shifted to lower temperatures (270 and 680 °C, respectively) compared to those of the Rh-0.8P catalyst. However, a remarkable reduction peak appeared at 350–400 °C in the TPR trace of the catalysts with higher P loadings (2.2–3.0 wt%). Brock et al. have reported that Rh_2P is formed by the reduction of rhodium phosphate at 375 °C [41]. Furthermore, Oyama et al. reported that one reduction peak in the TPR trace of a Ni_2P/SiO_2 catalyst with a higher P/Ni ratio

(P/Ni > 1) was observed to appear at the same temperature as that of a peak in the TPR trace of bulk nickel phosphate during reduction [21]. These results suggest that the large peak at 350–400 °C in the TPR traces of catalysts with higher P loadings (2.2–3.0 wt%) can be attributed to the reduction of rhodium phosphate.

The peaks for P_2O_5 and P_4O_7 appeared in the XRD pattern of a 20 wt% Ni_2P/SiO_2 catalyst with a higher P loading (P/Ni = 2) [25]. This result indicates that the particle size of the phosphate increases with increasing P loading. Thus, enlarged phosphate particles that weakly interact with SiO_2 would cause a peak shift to lower temperatures.

3. 2. 4. XRD Patterns of the Reduced Rh-xP Catalysts

The XRD patterns of the reduced Rh-xP catalysts were examined to evaluate the formed Rh_xP_y. **Figure 5** shows the XRD patterns of the Rh-xP catalysts reduced at 450–650 °C. The peaks for metallic Rh were only observed in the patterns of Rh catalysts reduced at any temperature. The same tendency was observed in the Rh-0.8P catalyst, but small peaks for Rh_2P appeared in the sample subjected to the highest reduction temperature (650 °C). The peaks for metallic Rh were observed in the

XRD patterns of the Rh-1.5 P catalyst reduced at 450 °C. However, these peaks disappeared when reduction temperature was increased, and Rh_2P peaks subsequently appeared. In addition, no metallic Rh peaks were observed in the Rh-xP catalysts with higher P loadings (greater than 2.2 wt%) reduced at any temperature. Thus, the TPR and XRD results indicated that Rh_2P is easily formed at higher P loadings and higher reduction temperatures. This phenomenon is can be explained as follows: the phosphate preferentially interacts with SiO_2, but excess phosphate interacts with Rh_2O_3 and/or forms rhodium phosphate. Because these phosphate species are reduced at lower temperatures than phosphates on SiO_2, Rh_2P is readily formed in the catalysts with higher P loadings. In contrast, the intensity of the Rh_2P peaks increased as the P loadings and reduction temperatures were increased. This result implies that excess P loading and a high reduction temperature cause sintering of Rh species. Furthermore, RhP_2 was formed in the catalyst with a higher P loading (3.0%) that that reduced at high temperature (650 °C).

Table 4 shows the effect of reduction temperature and P loading on the crystallite size of the metallic Rh and Rh_XP_Y, as calculated using

Scherrer's equation. The crystallite size of the Rh in the Rh catalyst increased with increasing reduction temperature. However, irrespective of the increase in reduction temperature from 550 to 650 °C, the crystallite size of the metallic Rh in the Rh-0.8P catalyst decreased. The same tendency was also observed in the other Rh-xP catalysts. Furthermore, the crystallite size of the RhP_2 was smaller than that in the Rh-3.0P catalyst reduced at 650 °C. At the same reduction temperature, the crystallite size of the Rh species increased with increasing P loading and increasing reduction temperature.

Bussell et al. have reported that the average crystallite size of Rh_2P in a 5 wt% Rh_2P/SiO_2 catalyst (P/Rh = 0.75) is 10 nm, as determined from its XRD pattern [40]. This value is higher than our results. Furthermore, the particle sizes of the Rh-xP catalysts were examined in detail using TEM.

3. 2. 5. Particle Size of the Reduced Rh-xP Catalysts

Figure 6 shows the TEM images of the Rh-xP catalysts after reduction at 550 °C. For the Rh catalyst, highly dispersed particles were observed. However, an increase in the P content tended to result in larger particle

sizes. The particle size distribution of the Rh-xP catalysts after reduction at 450–650 °C, as determined from TEM images, is shown in **Figure 7**. For the Rh catalyst, the particle size distribution shifted toward larger particle diameters as reduction temperature was increased. In particular, all of the Rh-xP catalysts reduced at 650 °C showed a low frequency of the peak center and a broad distribution compared to those reduced at 450 and 550 °C.

The average particle sizes of the Rh-xP catalysts reduced at 450–650 °C, as calculated from TEM images, are listed in **Table 5**. The average particle size of all of the Rh-xP catalysts reduced at 550 °C was slightly larger (+0.1-0.2 nm) than that of the catalysts reduced at 450 °C. For catalysts with P loadings less than 1.5 wt%, the average particle size of the catalysts reduced at 650 °C was 0.5-0.6 nm larger than that of the catalysts reduced at 550 °C. For catalysts with a P loading greater than 2.2 wt%, the average particle size of the catalysts reduced at 650 °C was 0.1-0.4 nm larger than that of the catalysts reduced at 550 °C, thereby indicating that excess P inhibits sintering of Rh_2P at 650 °C. However, at the same reduction temperature, the average particle size increased with

increasing P content. These results reveal that an excess P loading (greater than 2.2 wt%) leads to the formation of large particles. The BET surface area (**Table 2**) and TPR (**Fig. 4 (a)**) results imply that phosphate preferentially interacts with the SiO_2 support, but not with Rh_2O_3. Therefore, this phenomenon is can be explained as follows: The phosphate preferentially interacts with SiO_2, but excess phosphate interacts with Rh_2O_3 and forms rhodium phosphate. Since reduction of these phosphate species occur at lower temperature than that of phosphate on SiO_2, Rh_2P is readily formed in the catalysts with higher P loading.

Bussell et al. reported an average particle size of Rh_2P of 3.3 ± 1.7 nm, as determined from TEM images [40]. This particle size is smaller than the particle size indicated by our results, as shown in **Table 5**. In this work, the Rh loading was 5 wt%, and this loading was higher than that used by Bussell's group (Rh: 4.08 wt% and P: 0.92 wt%). Thus, our larger particle size can be explained by our higher Rh loading.

3. 2. 6. CO Uptake of Rh-xP Catalysts

Figure 8 shows the relationship between the reduction temperature and CO uptake of the Rh-xP catalysts. The CO uptake of the Rh-xP

catalysts decreased with an increase in reduction temperature. In particular, the CO uptake of the Rh-0.8P catalyst remarkably decreased as reduction temperature was increased from 600 to 650 °C. At higher reduction temperatures (greater than 600 °C), PO_4^{3-}, which interacts with SiO_2, can be reduced to form P and/or PH_3, as shown in **Fig. 4**. Thus, a remarkable decrease in the CO uptake of the Rh-0.8P catalyst can be explained by the metallic Rh surface being covered by P and/or the formation of Rh_2P.

At the same reduction temperature, the CO uptake decreased with increased P loading. These trends are consistent with the average particle sizes measured from TEM images (**Table 5**), but not with the crystallite sizes calculated from the XRD patterns (**Table 4**). The trend of the particle sizes calculated from the XRD results can be explained as follows: If phosphidation proceeds from the surface of the metallic Rh particles, then structures that consist of metallic Rh cores covered with Rh_2P shells would be formed. The size of the Rh cores would decrease as the degree of phosphidation increased. Thus, the crystallite size of metallic Rh decreased with increasing reduction temperature, as shown in

Table 4.

Oyama et al. have reported that the Ni_2P active phase is blocked by excess P in Ni_2P/SiO_2 catalysts with higher P contents [22]. In addition, we confirmed that RhP_2 is formed in the Rh-3.0P catalyst reduced at 650 °C (**Fig. 5**). These results imply that reduced excess P species cover the surface of the Rh_2P and/or react with Rh_2P to form RhP_2.

3. 2. 7. Turnover Frequency of the Rh-xP Catalysts

The turnover frequency of the Rh-xP catalysts was calculated from the amount of exposed Rh (Rh_{ex}) and from the CO uptake. The Rh_{ex} (mol g-cat^{-1}) values of the Rh-xP catalysts were calculated from their average particle size. Assuming that particles have a spherical or cubic shape, Rh_{ex} can be estimated from following equation:

$$Rh_{ex} = \frac{6nf}{\rho D N_A} \times 10^7 \quad (3)$$

where n is the surface atom density (atoms cm^{-2}), f is the fractional weight loading of the sample, ρ is the theoretical bulk density (g m^{-3}), D is the particle size calculated from TEM observations (nm), and N_A is Avogadro's number (6.02×10^{23}). The values of n were 1.60×10^{19} and 7.63×10^{19} atoms m^{-2} for Rh ((111) plane) and Rh_2P ((111) plane),

respectively. Furthermore, the values of ρ were 12.41 and 9.44 g cm^{-3} for Rh and Rh_2P, respectively. The calculated Rh_{ex} and chemisorbed CO/Rh_{ex} values are listed in **Table 6**. The CO/Rh_{ex} of the Rh catalyst reduced at any temperature was constant (ca. 1.7), indicating that CO species chemisorbed onto this catalyst would be dicarbonyl and linear types. However, the CO/Rh_{ex} of the Rh-0.8P catalyst decreased with increasing reduction temperature, especially from 550 to 650 °C. In other Rh-xP catalysts, CO/Rh_{ex} also decreased with increasing reduction temperature. Some CO species chemisorbed onto Rh_2P/Al_2O_3 catalysts, such as linear, bridge, and dicarbonyl types, have been identified by IR [42]. However, the CO/Rh_{ex} ratios for the Rh-xP catalysts with higher P loadings (greater than 2.2 wt%) were less than 1. These results can be explained by the exposed Rh sites of Rh_2P being covered by reduced P and/or by CO linearly adsorbing onto the Rh-xP catalysts because of steric hindrance caused by excess P.

Figure 9 shows the TOF values calculated from the Rh_{ex} (TOF (Rh_{ex})) and CO uptake (TOF (CO)) values. These TOFs varied in similar manners with increasing reduction temperature. The TOFs of the Rh catalyst

barely changed as reduction temperature was increased. Because the Rh catalyst exhibited a high CO/Rh_{ex} ratio (ca. 1.7), as shown in **Table 6**, the TOF (Rh_{ex}) would be more accurate than the TOF (CO). However, both TOFs calculated from both the Rh_{ex} **(a)** and CO uptake **(b)** of the Rh-0.8P catalyst increased as reduction temperature was increased from 550 to 650 °C. For the Rh-1.5P catalyst, the TOF (CO) also increased with increasing reduction temperature; however, the TOF (Rh_{ex}) slightly decreased with when reduction temperature was increased from 550 to 650 °C. Because the peak intensities of Rh_2P increased with increasing reduction temperature (**Fig. 5**), the enhancement of TOF was caused by Rh_2P formation. However, the TOFs of the Rh-2.2P catalyst decreased at reduction temperatures greater than 550 °C. The same trend was observed for the Rh-3.0P catalyst reduced at temperatures greater than 450 °C.

Figure 10 shows the TOFs of the Rh-xP catalysts as a function of their P loading. The TOFs were calculated from the maximum HDS activity (**Fig. 1**). In the P-loading range from 0 to 1.5, the TOF (Rh_{ex}) was the same as the TOF (CO). In contrast, a remarkable difference between these TOFs was observed in catalysts with higher P loadings (greater than

2.2 wt%). Furthermore, the CO/Rh_{ex} ratios of these catalysts were significantly lower than those of catalysts with low P contents (0-0.8 wt%) (**Table 6**). Thus, the TOFs of the Rh-xP catalysts with higher P loadings include an error caused by the Rh sites being covered by excess P.

The TOF of the Rh-1.5P catalyst reduced at 550 °C, which exhibited the highest HDS activity (Fig. 2), was approximately 200 h^{-1}. In the HDS of thiophene at 370 °C, the TOF of the Ni_2P/SiO_2 (P/Ni = 0.8) catalyst was ca. 76 h^{-1} (0.021 s^{-1}) [25]. The TOF of the Rh-1.5P catalyst was 2.6 times greater than that of the Ni_2P/SiO_2 catalyst.

3. 3. Effect of Reduction Temperature and P Loading on the HDS Activities of Rh-xP Catalysts

The TPR and XRD results revealed that an increase in the P content causes the reduction of phosphates at lower temperatures and decreases the formation temperature of Rh_2P. Thus, the reduction temperature for the maximum HDS activity decreased with increasing P loading, as shown in **Fig. 1**.

For the Rh-0.8P catalyst, the maximum HDS activity and a high TOF

were obtained at a high reduction temperature (650 °C). Bussell et al. have reported that the Rh_2P/SiO_2 catalyst, which exhibits metallic properties and excellent hydrogenation activity, showed higher sulfur tolerance than the Rh/SiO_2 catalyst [40]. In fact, we observed peaks associated with metallic Rh and small peaks associated with Rh_2P in the XRD pattern of the Rh-0.8P catalyst reduced at 650 °C (**Fig. 5**). Thus, the enhanced activity of the Rh-0.8P catalyst can be explained by the formation of a Rh_2P shell structure containing a metallic Rh core. When reduction temperature was increased to 700 °C, the HDS activity of the Rh-0.8P catalyst decreased. In addition, the HDS activities of other Rh-xP catalysts reduced at temperatures greater than 650 °C were lower than that of catalysts reduced at temperatures less than 550 °C. The TEM observations and CO adsorption results revealed that the average metallic Rh and Rh_2P particle sizes increased as reduction temperature was increased from 550 to 650 °C. Therefore, the low HDS activities of the Rh-xP catalysts reduced at higher temperatures were due to sintering of the metallic Rh and Rh_2P particles. In addition, the HDS activity of the Rh-3.0P catalyst reduced at temperatures greater than 600 °C was lower

than that of the Rh catalyst reduced at the same temperature (**Fig. 1**). The XRD analysis showed that excess P reacts with Rh_2P to form RhP_2 in the Rh-3.0P catalyst reduced at 650 °C (**Fig. 5**). Metal-rich phosphides exhibit excellent hydrogenation activity [3], and Ni-rich phosphides exhibit much higher HDS activity than P-rich phosphides [24]. Korányi have reported that Ni_2P catalysts exhibit greater activity than NiP_2 catalysts [23]. For Ni_2P catalysts, the Ni(1) sites with tetrahedral coordination and four nearest-neighbor P atoms are responsible for direct desulfurization, whereas the Ni(2) sites with square pyramidal coordination and five nearest-neighbor P atoms are highly active sites for the hydrogenation route [28]. Furthermore, DFT calculation results have shown that P sites play an important role in the bonding of intermediates, such as H adatoms [18]. Because the coordination number of Rh-P in RhP_2 is greater than that in Rh_2P, Rh_2P favors the hydrogenation route to form THT. The Rh-3.0P catalyst exhibited remarkably lower CO/Rh_{ex} ratios compared to those of the Rh-xP catalysts with low P loadings (less than 1.5 wt%), indicating that the Rh sites were covered by excess P. Thus, the low HDS activity and remarkable THT selectivity of the

Rh-3.0P catalysts reduced at higher temperatures (**Table 1 and 2**) resulted from the formation of RhP_2 and from a decrease in the number of active sites for C-S bond cleavage due to the coverage by excess P.

The optimal P loading for HDS activity of the Rh-xP catalysts was 1.5 wt%, as shown in **Fig. 2**. This result is explained as follows: At a lower P loading (0.8 wt %), a small amount of Rh_2P formed at high reduction temperatures; however, a metallic Rh phase was also observed (**Fig. 5**), indicating that the degree of phosphidation was low compared with that of catalysts with high P loadings. Furthermore, the high reduction temperature simultaneously causes sintering of the active phase, as shown in **Table 5** and in **Fig. 8**. In contrast, Rh_2P was easily formed at low reduction temperatures in the catalysts with higher P loadings (greater than 2.2 wt %). However, the results of TEM observations and CO adsorption experiments showed that excess P causes aggregation and/or covering of Rh_2P. Because moderate P loadings lead to the formation of well-dispersed Rh_2P at a relatively low temperature (550 °C), the Rh-1.5P catalyst exhibited the highest HDS activity.

4. Conclusions

The effect of reduction temperature and P loading on the formation of active sites and on the HDS activity of Rh-xP/SiO_2 catalysts was investigated. Reduction temperature strongly affects the HDS activities of Rh-xP catalysts, and the optimal reduction temperature for maximum HDS activity decreased with increasing P content. The Rh-1.5P catalyst exhibited the highest HDS activity—four times higher than that of the Rh catalyst. Analysis of the TPR and XRD patterns of the Rh-xP catalysts revealed that the formation temperature of Rh_2P decreases with increased P loading. Furthermore, the formation of RhP_2 was observed in the Rh-3.0P catalyst after it was reduced at higher temperatures. Average particle size calculated from TEM images increased and CO uptake decreased with increased P loading. Thus, we concluded that a moderate P loading, which resulted in good reducibility of the phosphates and a small Rh_2P particle size, caused the high HDS activity of the Rh-1.5P catalyst.

Acknowledgment

We would like to thank Nippon Aerosil Co. for supplying the silica.

This work was supported by a Grant-in-Aid for Young Scientists (B), Japan (21750158).

References

[1] Y. Okamoto, Catal. Today 132 (2008) 9-17.

[2] S.T. Oyama, T. Gott, H. Zhao, Y.K. Lee, Catal. Today 143 (2009) 94-107.

[3] R. Prins, M.E. Bussell, Catal. Lett. 142 (2012) 1413-1436.

[4] Y. Okamoto, K. Ochiai, M. Kawano, T. Kubota, J. Catal. 222 (2004) 143-151.

[5] Y. Okamoto, Catal. Today 132 (2008) 9-17.

[6] N. Rinaldi, Usman, K. Al-Dalama, T. Kubota, Y. Okamoto, Appl. Catal. A: Gen. 360 (2009) 130-136.

[7] T. Fujikawa, Catal. Surv. Asia 10 (2006) 89-97.

[8] Usman, T. Yamamoto, T. Kubota, Y. Okamoto, Appl. Catal. A, Gen. 328 (2007) 219-225.

[9] M. Sugioka, F. Sado, T. Kurosaka, X. Wang, Catal. Today 45 (1998) 327-334.

[10] Y. Kanda, T. Kobayashi, Y. Uemichi, S. Namba, M. Sugioka, Appl. Catal. A: Gen. 308 (2006) 111-118.

[11] A. Niquille-Röthlisberger, R. Prins, Catal. Today 123 (2007) 198-207.

[12] Y. Kanda, A. Seino, T. Kobayashi, Y. Uemichi, M. Sugioka, J. Jpn. Petrol. Inst. 52 (2009) 42-50.

[13] A.M. Venezia, R. Murania, V. La Parola, B. Pawelec, J.L.G. Fierro, Appl. Catal. A: Gen. 383 (2010) 211-216.

[14] Z. Vít, D. Gulková, L. Kaluža, S. Bakardieva, M. Boaro, Appl. Catal. B: Environ. 100 (2010) 463-471.

[15] P.A. Aegerter, W.W.C. Quigley, G.J. Simpson, D.D. Ziegler, J.W. Logan, K.R. McCrea, S. Glazier, M.E. Bussell, J. Catal. 164 (1996) 109-121.

[16] B. Dhandapani, T.St. Clair, S.T. Oyama, Appl. Catal. A Gen. 168 (1998) 219-228.

[17] M. Lewandowski, A. Szymańska-Kolasa, P. Da Costa, C. Sayag, Catal. Today 119 (2007) 31-34.

[18] P. Liu, J.A. Rodriguez, T. Asakura, J. Gomes, K. Nakamura, J. Phys.

Chem. B 109 (2005) 4575-4583.

[19] M. Nagai, Appl. Catal. A: Gen. 322 (2007) 178-190.

[20] C. Stinner, Z. Tang, M. Haouas, Th.Weber, R. Prins, J. Catal. 208 (2002) 456-466.

[21] S.T. Oyama, X.Wang, Y.K. Lee, K. Bando, F.G. Requejo, J. Catal. 210 (2002) 207-217.

[22] S.J. Sawhill, D.C. Philips, M.E. Bussell, J. Catal. 215 (2003) 208-219.

[23] T.I. Korányi, Appl. Catal. A: Gen. 239 (2003) 253-267.

[24] A. Wang, L. Ruan, Y. Teng, X. Li, M. Lu, J. Rena, Y. Wang, Y. Hu, J. Catal. 229 (2005) 314-321.

[25] S.J. Sawhil, K.A. Layman, D.R. Van Wyk, M.H. Engelhard, C. Wang, M.E. Bussell, J. Catal. 231 (2005) 300-313.

[26] S. Yang, C. Liang, R. Prins, J. Catal. 237 (2006) 118-130.

[27] Y.K. Lee, S.T. Oyama, Appl. Catal. A: Gen. 322 (2007) 191-204.

[28] S.T. Oyama, Y.K. Lee, J. Catal. 258 (2008) 393-400.

[29] E. Muthuswamy, G.H.L. Savithra, S.L. Brock, ACS Nano 5 (2011) 2402-2411.

[30] S.T. Oyama, J. Catal. 216 (2003) 343-352.

[31] J.A. Rodriguez, J.Y. Kim, J.C. Hanson, S.J. Sawhill, M.E. Bussell, J. Phys. Chem. B, 107 (2003) 6276-6285.

[32] P. Clark, X. Wang, S.T. Oyama, J. Catal. 207 (2002) 256-265.

[33] D.C. Phillips, S.J. Sawhill, R. Self, M.E. Bussell, J. Catal. 207 (2002) 266-273.

[34] P.A. Clark, S.T. Oyama, J. Catal. 218 (2003) 78-87.

[35] A. Montesinos-Castellanos, T.A. Zepeda, B. Pawelec, J.L.G. Fierro, J.A. de los Reyes, Chem. Mater. 19 (2007) 5627-5636.

[36] A. Montesinos-Castellanos, T.A. Zepeda, B. Pawelec, E. Lima, J.L.G. Fierro, A. Olivas, J.A. de los Reyes H., Appl. Catal. A: Gen. 334 (2008) 330-338.

[37] Y. Kanda, C. Temma, K. Nakata, M. Sugioka, Y. Uemichi, Appl. Catal. A: Gen. 386 (2010) 171-178.

[38] Y. Kanda, K. Nakata, C. Temma, M. Sugioka, Y. Uemichi, J. Jpn. Petrol. Inst. 55 (2012) 108-119.

[39] Y. Kanda, T. Ichiki, S. Kayaoka, A. Sawada, M. Sugioka, Y. Uemichi, Chem. Lett. 42 (4) (2013) 404-406.

[40] J.R. Hayes, R.H. Bowker, A.F. Gaudette, M.C. Smith, C.E. Moak, C.Y. Nam, T.K. Pratum, M.E. Bussell, J. Catal. 276 (2010) 249-258.

[41] C.M. Sweeney, K.L. Stamm, S.L. Brock, J. Alloys Comp. 448 (2008) 122-127.

[42] S. Cimino, G. Mancino, L. Lisi, Appl. Catal. B: Environ. 138-139 (2013) 342-352.

Figure captions

Figure 1 Relationship between the reduction temperature and HDS activity of Rh-xP catalysts.

Figure 2 Effect of P loading on the HDS activity of Rh-xP catalysts reduced at an optimal temperature.

Figure 3 XRD patterns of Rh-xP catalysts calcined at 500 °C.

Figure 4 TPR of Rh-xP catalysts: (a) TPRs of Rh-xP and Rh/SiO_2 + P/SiO_2 mixed catalysts (0.05 + 0.05 g) from 30 to 800 °C and (b) a magnified version of the 200 to 800 °C region of the TPR trace.

Figure 5 XRD patterns of Rh-xP catalysts reduced at 450–650 °C.

Figure 6 TEM images of Rh-xP catalysts reduced at 550 °C.

Figure 7 Particle size distribution of Rh-xP catalysts reduced at 450–650 °C.

Figure 8 Relationship between the reduction temperature and CO uptake of Rh-xP catalysts.

Figure 9 Relationship between the reduction temperature and TOF of Rh-xP catalysts calculated from (a) the theoretical number of exposed Rh atoms and (b) the CO uptake.

Figure 10 Effect of P loading on the TOF of Rh-xP catalysts calculated from the theoretical number of exposed Rh atoms and CO uptake.

Table 1 Selectivities of reaction products in the HDS of thiophene over Rh-xP catalysts. Reaction conditions: W/F = 37.9 g h mol^{-1}, H_2/C_4H_4S = 30, total pressure = 0.1 MPa.

Catalyst	Reduction temperature (°C)	Conversion (%)	Selectivity of HDS products (%)				TOF (h^{-1})	
			C_1-C_3[a]	Butanes	Butenes	THT[b]	Rh_{ex}[c]	CO[d]
Rh	450	16.6	0.3	10.3	86.2	3.2	35.5	20.5
	550	16.8	0.3	9.9	86.4	3.3	36.5	20.9
	650	16.3	0.2	10.2	86.1	3.6	39.5	23.4
Rh-0.8P	450	26.6	0.0	21.8	77.1	1.1	64.1	41.8
	550	27.9	0.0	15.8	81.2	3.0	68.6	49.5
	650	44.4	0.0	18.5	78.1	3.4	119	113
Rh-1.5P	450	43.2	0.3	22.0	74.5	3.4	152	137
	550	55.0	0.1	20.8	75.6	3.5	200	202
	650	43.1	0.1	14.4	81.0	4.3	171	230
Rh-2.2P	350	48.3	0.2	21.2	74.9	3.7	-	197
	450	47.8	0.3	21.4	73.1	5.2	211	300
	550	45.4	0.2	21.4	72.6	5.9	204	312
	650	27.3	0.1	12.6	75.6	11.7	129	204
Rh-3.0P	350	34.0	0.2	11.8	81.4	6.6	138	279
	450	29.3	0.0	13.1	74.7	12.2	143	360
	550	14.2	0.4	9.9	72.4	17.3	70.4	147
	650	7.49	0.5	5.0	75.4	19.0	38.7	118

a C_1-C_3 hydrocarbons

b Tetrahydrothiophene

c Calculated from the theoretical number of exposed Rh atoms

d Calculated from the CO uptake

Table 2 Effect of W/F on selectivities of reaction products in the HDS of thiophene over Rh-xP catalyst reduced at 650°C. Reaction conditions: W = 0.003-0.1 g, H_2/C_4H_4S = 30, total pressure = 0.1 MPa.

Catalyst	W/F (g h mol^{-1})	Conversion (%)	Selectivity of HDS products (%)			
			C_1-C_3[a]	Butanes	Butenes	THT[b]
Rh	15.2	7.81	4.4	5.8	86.1	3.3
	37.9	16.3	0.2	10.2	86.1	3.6
Rh-1.5P	1.1	10.4	1.6	4.7	78.2	15.5
	3.8	20.8	0.2	7.5	80.6	11.8
	7.6	30.8	0.4	11.0	80.7	8.0
	37.9	43.1	0.1	14.4	81.0	4.3
Rh-3.0P	37.9	7.49	0.5	5.0	75.4	19.0

a C_1-C_3 hydrocarbons

b Tetrahydrothiophene

Table 3 BET surface area and crystallite size of Rh-xP catalysts after calcination.

Catalyst	BET surface area (m^2 g^{-1})	Crystallite size (nm)	
		Rh_2O_3	Rh
Rh	289	1.2	-
Rh-0.8P	258	1.6	-
Rh-1.5P	249	1.9	-
Rh-2.2P	222	6.6	14.4
Rh-3.0P	215	-	15.7

Table 4 Crystalline size of Rh species calculated by Scherrer's equation in XRD patterns of Rh-xP catalysts after reduction.

	Crystallite size of Rh / Rh_2P / RhP_2 (nm)			
Reduction temperature	350 °C	450 °C	550 °C	650 °C
Catalyst				
Rh	- / - / -	2.6 / - / -	2.6 / - / -	3.2 / - / -
Rh-0.8P	- / - / -	3.1 / - / -	3.8 / - / -	3.5 / 2.2 / -
Rh-1.5P	- / - / -	6.7 / 3.3 /-	6.4 / 6.1 /-	- / 7.7 /-
Rh-2.2P	- / - / -	- / 8.9 / -	- / 9.9 / -	- / 9.3 / -
Rh-3.0P	- / 12.2 / -	- / 9.4 / -	- / 13.2 / -	- / 12.7 / 10.9

Table 5 Average particle diameter of Rh-xP catalysts after reduction measured from TEM images.

	Average particle size (nm)			
Reduction temperature	350 °C	450 °C	550 °C	650 °C
Catalyst				
Rh	-	5.2	5.3	5.9
Rh-0.8P	-	5.9	6.0	6.5
Rh-1.5P	-	6.2	6.4	7.0
Rh-2.2P	-	7.7	7.9	8.3
Rh-3.0P	7.1	8.7	8.8	8.9

Table 6 The theoretical number of exposed Rh atoms (Rh_{ex}) and CO/Rh_{ex} of reduced Rh-xP catalysts.

Catalyst	Reduction temperature (°C)	Rh species for Rh_{ex} calculation (The most intense peak of XRD)	Rh_{ex} (μmol g-cat^{-1})	CO/Rh_{ex}[a]
Rh	450	Rh	123	1.74
	550	Rh	121	1.75
	650	Rh	109	1.69
Rh-0.8P	450	Rh	109	1.54
	550	Rh	108	1.38
	650	Rh	71	1.47
Rh-1.5P	450	Rh_2P	75	1.10
	550	Rh_2P	73	0.99
	650	Rh_2P	66	0.75
Rh-2.2P	450	Rh_2P	60	0.70
	550	Rh_2P	59	0.65
	650	Rh_2P	56	0.63
Rh-3.0P	350	Rh_2P	65	0.41
	450	Rh_2P	54	0.40
	550	Rh_2P	53	0.52
	650	Rh_2P	51	0.33

a CO uptake/the theoretical number of exposed Rh atoms ratio

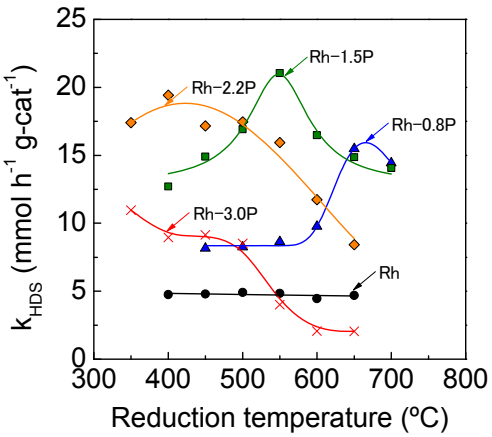
25
20
15
10
5
0
300
400
500
600
700
800
k_{HDS} (mmol h^{-1} $g\text{-}cat^{-1}$)
Reduction temperature (ºC)
Rh−1.5P
Rh−2.2P
Rh−0.8P
Rh−3.0P
Rh

Fig. 1

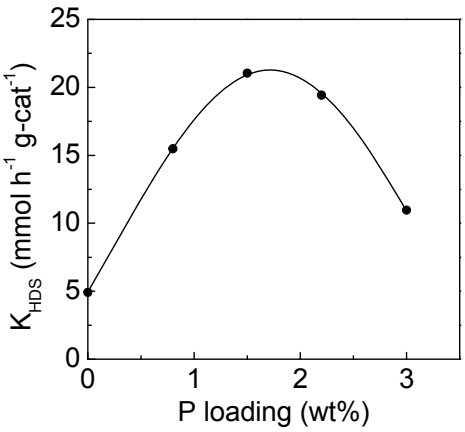

Fig. 2

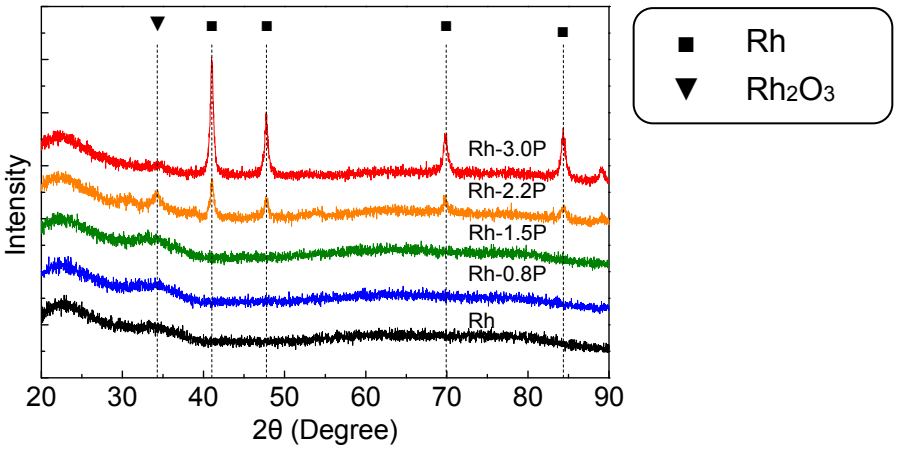
Rh
Rh2O3
Rh-3.0P
Rh-2.2P
Rh-1.5P
Rh-0.8P
Rh
Intensity
20
30
40
50
60
70
80
90
2θ (Degree)

Fig. 3

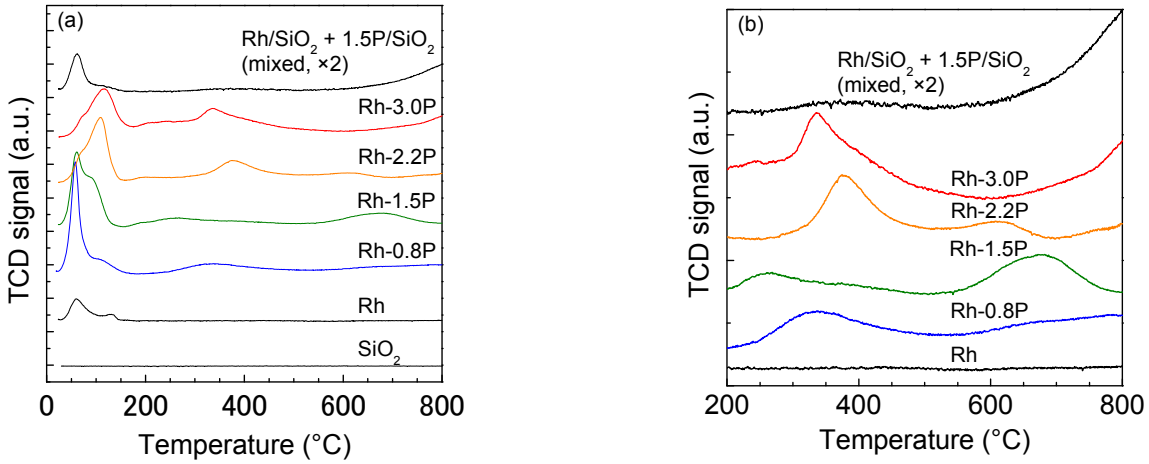
(a)
Rh/SiO2 + 1.5P/SiO2
(mixed, ×2)
Rh-3.0P
Rh-2.2P
Rh-1.5P
Rh-0.8P
Rh
SiO2
TCD signal (a.u.)
0
200
400
600
800
Temperature (°C)
(b)
Rh/SiO2 + 1.5P/SiO2
(mixed, ×2)
Rh-3.0P
Rh-2.2P
Rh-1.5P
Rh-0.8P
Rh
TCD signal (a.u.)
200
400
600
800
Temperature (°C)

Fig. 4

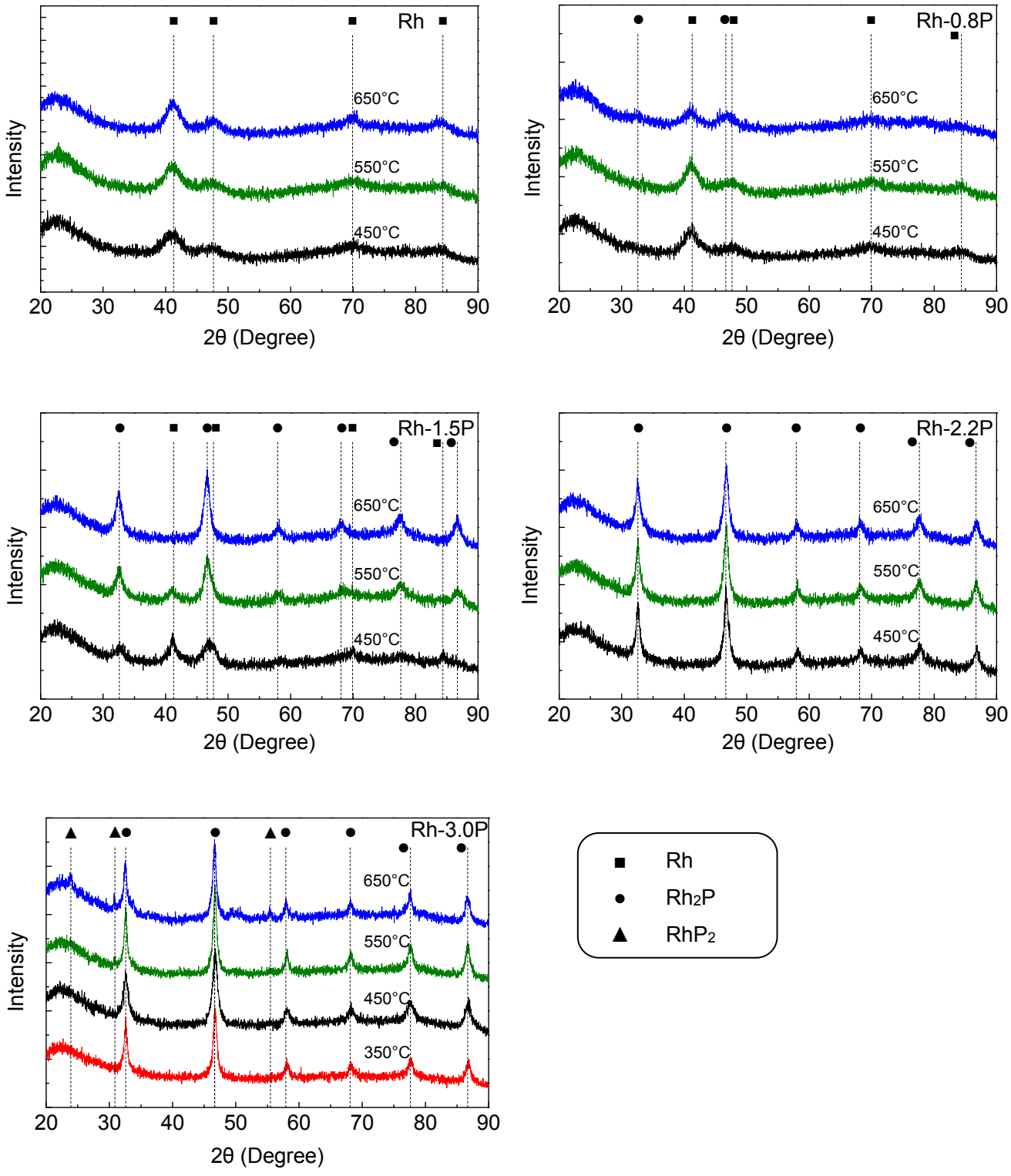
Rh
650°C
550°C
450°C
Intensity
2θ (Degree)
Rh-0.8P
650°C
550°C
450°C
Intensity
2θ (Degree)
Rh-1.5P
650°C
550°C
450°C
Intensity
2θ (Degree)
Rh-2.2P
650°C
550°C
450°C
Intensity
2θ (Degree)
Rh-3.0P
650°C
550°C
450°C
350°C
Intensity
2θ (Degree)
Rh
Rh2P
RhP2

Fig. 5

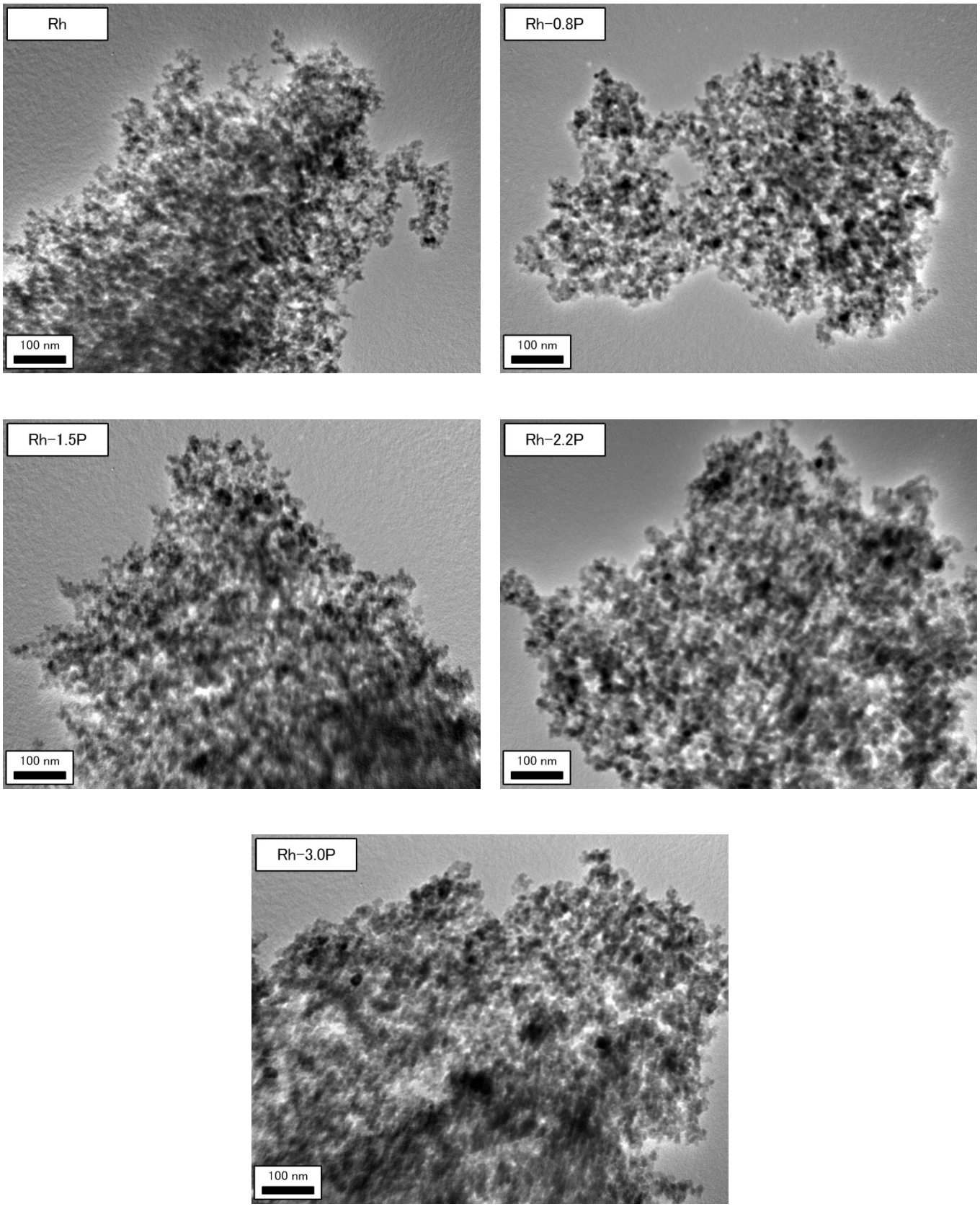

Fig. 6

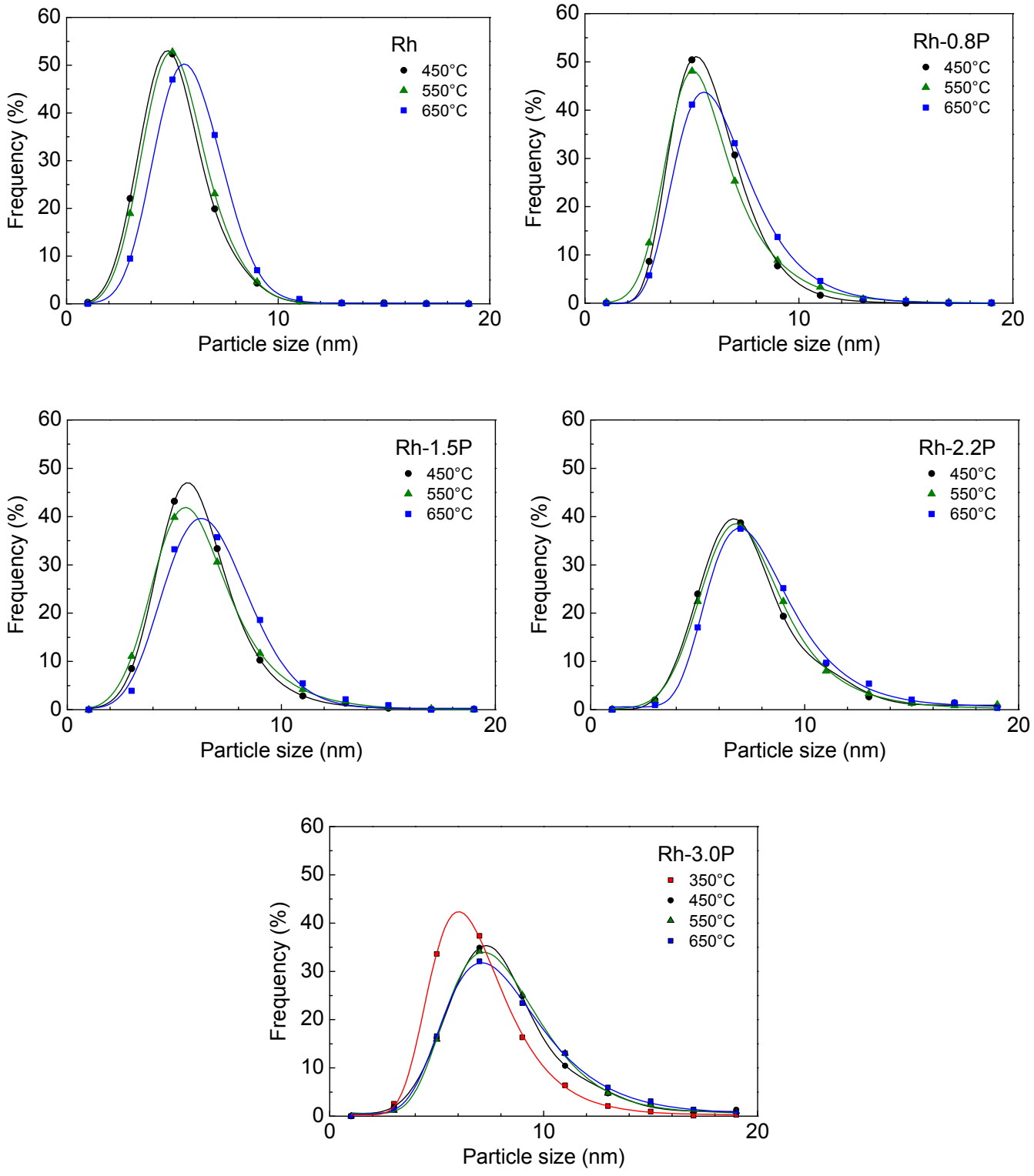
Rh
450°C
550°C
650°C
Rh-0.8P
450°C
550°C
650°C
Rh-1.5P
450°C
550°C
650°C
Rh-2.2P
450°C
550°C
650°C
Rh-3.0P
350°C
450°C
550°C
650°C
Frequency (%)
Particle size (nm)
0
10
20
30
40
50
60

Fig. 7

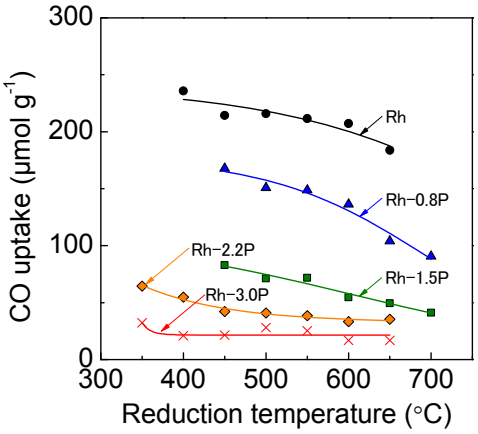
CO uptake (μmol g-1)
Reduction temperature (°C)
Rh
Rh−0.8P
Rh−1.5P
Rh−2.2P
Rh−3.0P
0
100
200
300
300
400
500
600
700

Fig. 8

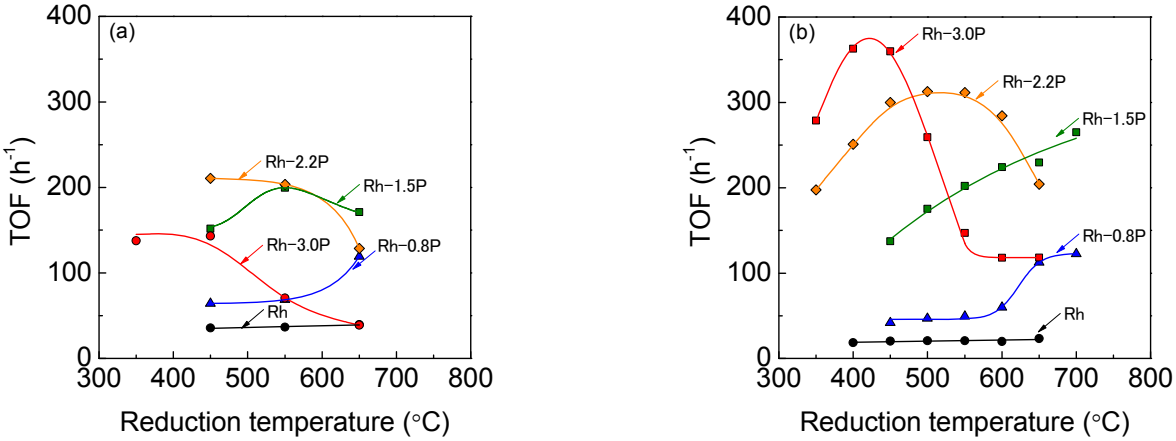
(a)
TOF (h-1)
Reduction temperature (°C)
Rh−2.2P
Rh−1.5P
Rh−3.0P
Rh−0.8P
Rh
(b)
TOF (h-1)
Reduction temperature (°C)
Rh−3.0P
Rh−2.2P
Rh−1.5P
Rh−0.8P
Rh

Fig. 9

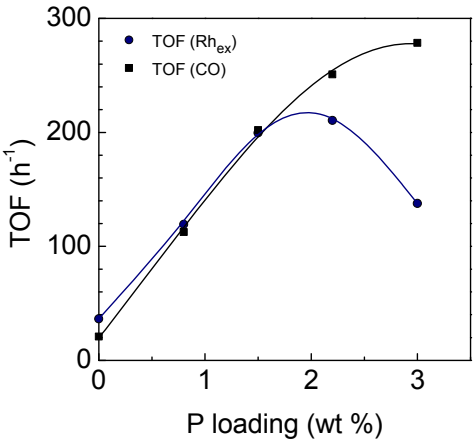

Fig. 10